

by the publisher

arXiv:1303.2050v1 [cond-mat.str-el] 8 Mar 2013

# Mott-Hubbard transition in $V_2O_3$ revisited

P. Hansmann<sup>1,2</sup>, A. Toschi<sup>1</sup>, G. Sangiovanni<sup>1,3</sup>, T. Saha-Dasgupta<sup>4</sup>, S. Lupi<sup>5</sup>, M. Marsi<sup>6</sup>, K. Held<sup>1</sup>

<sup>1</sup> Institute of Solid State Physics, Vienna University of Technology, 1040 Vienna, Austria

<sup>2</sup> Centre de Physique Théorique, École Polytechnique, CNRS, 91 128 Palaiseau, France

<sup>3</sup> Institut für Theoretische Physik und Astrophysik, Universität Würzburg, Am Hubland, D-97074 Würzburg, Germany

<sup>4</sup> S.N. Bose National Centre for Basic Sciences, Kolkata 700098, India

<sup>5</sup> CNR-IOM and Dipartimento di Fisica, Università di Roma "La Sapienza", Piazzale A. Moro 2, I-00185 Roma, Italy

<sup>6</sup> Laboratoire de Physique des Solides, CNRS-UMR 8502, Université Paris-Sud, F-91405 Orsay, France

Received XXXX, revised XXXX, accepted XXXX

Published online XXXX

**Key words:** Strongly correlated electron systems, Mott-Hubbard transition, vanadium sesquioxide, dynamical mean field theory.

\* Corresponding author:

The isostructural metal-insulator transition in Cr-doped  $V_2O_3$  is the textbook example of a Mott-Hubbard transition between a paramagnetic metal and a paramagnetic insulator. We review recent theoretical calculations as well as experimental findings which shed new light on this famous transition. In particular, the old paradigm of a doping-pressure equivalence does not hold, and there is a microscale phase separation for Cr-doped  $V_2O_3$ .

Copyright line will be provided by the publisher

**1 The story so far** At first, let us summarize the basic facts and review some of the former theoretical work that has been put forward, thereby also defining the necessary terms. In Fig. 1 we show the phase diagram of  $V_2O_3$  [2] spanned in the temperature–doping space displaying three phases: At ambient conditions  $V_2O_3$  is a paramagnetic metal (PM) and crystallizes in the corundum structure with four vanadium atoms in the primitive unit cell, see inset of Fig. 1. It can be seen that respectively two vanadium atoms form “pairs” which are oriented along the crystallographic  $c$ -axis. Upon cooling below  $\sim 150$ K, a peculiar antiferromagnetic order (AF) sets in and the system becomes insulating, accompanied by a monoclinic structural distortion. On the other hand, the system can be tuned by doping with chromium or titanium or the application of external pressure. In this respect, the “common wisdom” has been established [2] that doping and pressure can be seen as equivalent routes through the phase diagram. As we will see later, however, the pressure/doping equivalence scheme is inconsistent with recent experimental measurements of the optical conductivity and  $x$ -ray absorption. Above the Néel, temperature, the corundum crystal structure remains unchanged as a function of pressure or doping. Nonetheless, upon Cr doping a first order isostructural metal-to-

insulator (MIT) transition takes place (see Fig. 1) which evoked several theoretical attempts to describe this MIT as a genuine Mott–Hubbard transition. While the MIT is associated to changes in the lattice structure and the atomic positions [3,4], it is important to notice that  $x$ -ray diffraction showed that for a given temperature the structure within one phase *does not change upon doping* [4]. It was later also observed by Park *et al.* [5] with vanadium  $L$ -edge  $x$ -ray absorption spectroscopy that this holds also the electronic configuration of the system in terms of the orbital occupation (see Table 1 of [5]). Therefore we shall adopt the nomenclature of Robinson [4] and refer to the lattice structure of the paramagnetic metallic (PM) and insulating (PI) phase *at ambient pressure* as  $\alpha$ - and  $\beta$ -phase respectively.

The electronic configuration of atomic vanadium is  $[Ar]3d^34s^2$ , which means, that in the three-valent oxidation state we find a  $3d^2$  configuration realized. In the corundum type structure the vanadium atoms are coordinated by oxygen ligands in a trigonally distorted octahedral fashion (inset of Fig. 1). Hence, the cubic part of the crystal field splits the  $d$ -states into the lower lying  $t_{2g}$  and the

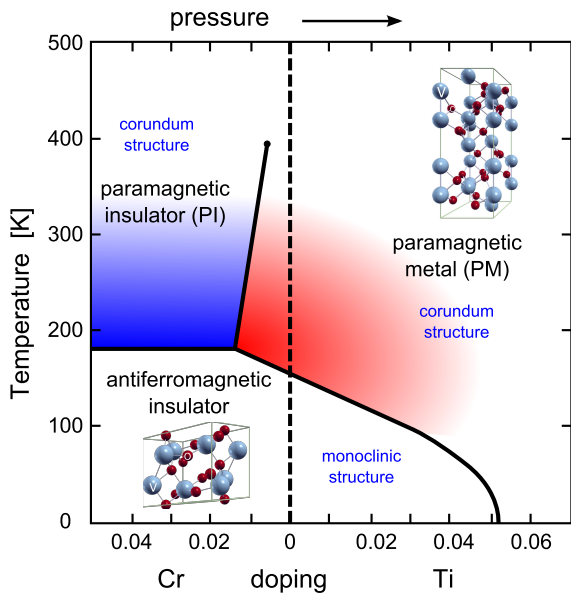


**Figure 1** (Color online) Temperature vs. doping phase diagram of  $V_2O_3$  according to [1]. In the PM and PI phase the compound crystallizes in the corundum structure, whereas the low temperature AF phase shows a monoclinic lattice structure. The double x-axis as pressure and doping reflects the paradigm of pressure-doping equivalence [2]. The monoclinic and corundum structure unit cells are shown as small insets.

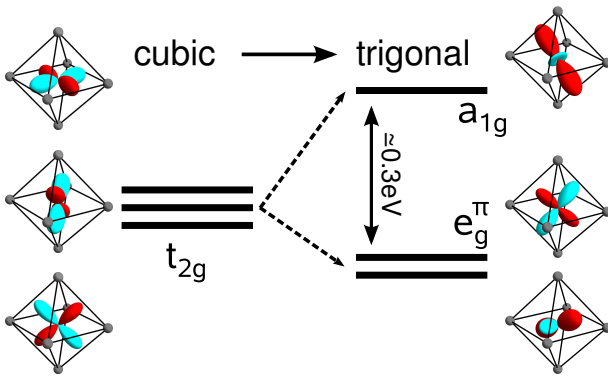


**Figure 2** (Color online) Level splitting of the vanadium  $t_{2g}$ -states: due to the trigonal distortion the  $t_{2g}$ -states split up in an  $e_g^\pi$  doublet and an  $a_{1g}$  singlet at a higher energy. From LDA results we estimate approximately 0.3 eV for this splitting. The plotted orbitals are spherical harmonic functions which display the symmetry of the states. These plots nicely compare to the NMTO Wannier function plots of Saha-Dasgupta *et al.* [6] (reprinted with permission from [7] Copyright (2012) by the American Physical Society).

higher lying  $e_g$  states. The trigonal distortion<sup>1</sup> acts like a compression along one of the three-fold axes of the octahedron (i.e. squeezing two opposite sides together). As a result the degeneracy of the lower lying  $t_{2g}$  states is lifted and they are split into a single  $a_{1g}$  and the twofold degenerate  $e_g^\pi$  states. This level splitting, together with a plot of the respective angular part of the (atomic) wave function, is sketched in Fig. 2. To indicate the difference to the  $t_{2g}$  states, the higher lying cubic  $e_g$  states (which are not split by the trigonal distortion) get an additional index  $e_g^\sigma$  in order to distinguish them from the  $e_g^\pi$ . The  $\sigma$  accounts for their orientation towards the ligands, with which they form  $\sigma$  bonds.

Since the  $e_g^\sigma$  are pushed up in energy by the crystal field, the two vanadium d-electrons populate the three  $t_{2g}$  levels. One of the crucial aspects concerning the understanding of the MIT is the specific occupation of these  $t_{2g}$  states. In an early work, Castellani *et al.* [8,9,10] assumed a strong hybridization of the V-V pairs oriented parallel to the rhombohedral c-axis, resulting in a strong bonding and antibonding splitting of the  $a_{1g}$  states. In this case, with the bonding states filled there would be one electron remaining in the twofold degenerate  $e_g^\pi$  states and the compound could be described by a quarter filled  $S = 1/2$  Hubbard model. However, later experimental evidence demonstrated [11, 12, 13, 5] that the ground state of the system is more complicated and should rather be described as a  $S = 1$  state consisting of a mixture of  $a_{1g}$  and  $e_g^\pi$  electrons.

Moreover, it is precisely the coefficients in the linear combination of  $a_{1g}$  and  $e_g^\pi$  for the ground state which allow for a quantitative distinction of the PM, PI, and AF phases. The XAS vanadium L-edge study of Park *et al.* explored the phase diagram by means of temperature and doping and summarized the respective ratio of  $e_g^\pi e_g^\pi$  to  $a_{1g} e_g^\pi$  occupations as [5]: 1:1 (PM), 3:2 (PI), and 2:1 (AF). As we mentioned earlier, their results turned out to be consistent with the x-ray diffraction data for the lattice of Robinson [4], and showed that, within the PM  $\alpha$ - and the PI  $\beta$ - phase, there is essentially no change in the ground state composition for different doping levels. One main new result, which will be discussed later, is, that this is not true for the pressurized metallic phase.

**LDA calculations** First *ab initio* band structure calculations in the local density approximation (LDA) for  $V_2O_3$  were performed by Mattheiss [14]. Not surprisingly the results neither captured the insulating character of the Cr doped PI phase nor the signatures of the strongly correlated character of the undoped PM phase (for example the photoemission spectral weight identified with the lower

<sup>1</sup> Let us, already in this introduction, remark that the actual crystal field breaks one significant point symmetry on the vanadium sites, namely inversion in the c-direction. This is related to the different distances of the neighboring vanadium atoms along the c-axis, see Fig. 1. While this effect is negligible for most of the discussion, it will be of great importance for the selection rules of the polarization dependent XAS results later on.

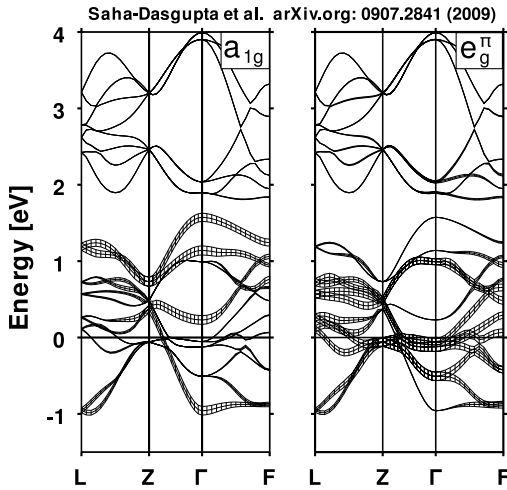


**Figure 3**  $V_2O_3$  bandstructure from LDA with “fat bands” indicating the orbital character. Left:  $a_{1g}$ ; right:  $e_g^\pi$  orbital character. (taken from Saha–Dasgupta *et al.* [6])

Hubbard band). Yet, even at the LDA level, some valuable information can be obtained. In Fig. 3, a plot of the LDA band structure is shown in the rhombohedral representation taken from Saha–Dasgupta *et al.* [6] with Fermi level  $\varepsilon_F = 0$ . In the two panels the respective  $a_{1g}$  and  $e_g^\pi$  character is indicated by the width of the lines by means of the so called “fat band” representation.

First of all it can be seen in Fig. 3 that the  $t_{2g}$  part is nicely separated from the rest of the bands: Genuine oxygen  $p$ -bands are lower lying than the displayed energy range and the  $e_g^\sigma$  can be identified as the bands at  $\approx 2$  eV to 4 eV.

Let us now turn to the  $a_{1g}$  bands (left panel Fig. 3). The previously mentioned bonding–antibonding splitting due to the V–V pairs can be seen at the  $\Gamma$ -point to be  $\gtrsim 2$  eV, where the  $a_{1g}$ -character is pure. The strongest dispersion is observed along the  $\Gamma$ - $Z$  direction where the main contribution stems from  $a_{1g}$ - $a_{1g}$  hopping. However, the dispersion of the  $a_{1g}$ -bands along the other directions is also not small which is a consequence of  $a_{1g}$ - $e_g^\pi$  hybridization. While the  $a_{1g}$  and  $e_g^\pi$  states are orthogonal eigenstates *locally* in a trigonal crystal field they still hybridize in a *non-local* way, i.e., there is intersite  $a_{1g}$ - $e_g^\pi$  hopping also in the  $ab$ -plane. As it was remarked by Elfimov *et al.* [15] these kinds of hopping are important for the shape of the  $a_{1g}$  states. With the help of the fat bands in Fig. 3, we compare the  $a_{1g}$  and  $e_g^\pi$ -character: We clearly see that only at the high symmetry points in the Brillouin zone the non-local  $a_{1g}$ - $e_g^\pi$  hybridization is zero. In fact, this LDA result contradicts also theoretically the validity of quarter filled  $e_g^\pi$  states and the  $S = 1/2$  scenario.

**Previous LDA+DMFT studies** By means of dynamical mean field theory (DMFT) [16] it is possible to include local electronic correlations, which trigger a Mott-Hubbard transition. Starting from the LDA results, first LDA+DMFT calculations were performed and compared

to photoemission and XAS experiments by Held *et al.* [17] and Keller *et al.* [18]. Later Poteryaev *et al.* [19] performed new LDA+DMFT calculations employing a downfolded NMTO  $t_{2g}$  Wannier functions Hamiltonian provided by Saha–Dasgupta *et al.* [6] instead of the density of states [17,18]. Both kind of LDA+DMFT calculations capture the Mott-Hubbard transition, and well agree with (even predicted) the photoemission spectroscopy (PES) measurements. Actually, the PES spectra at the time of the first calculations [17] still did not show a pronounced quasi-particle peak [20]. Only after improving the bulk sensitivity by using high-energy photons from a synchrotron source [21,22], experiments agreed also in this respect with LDA+DMFT.

Extending the work of Poteryaev *et al.* [19], Tomczak [23] and Tomczak and Biermann [24] discussed the optical conductivity of the compound introducing corrections for the calculation of the Fermi-velocities associated with the non-monoatomic basis of  $V_2O_3$  – an important issue also for this work which will be discussed in the next section. The last work that should be mentioned is the joint experimental/theory paper by Baldassare *et al.* [25] in which the authors show that the slight change of the lattice parameters due to temperature, drive the system into the crossover regime between metal and insulator. Their results underline how sensitive strongly correlated systems are with respect to the change of external parameter – even more so in the vicinity of a correlation driven Mott transition. For a comparison to other vanadium oxides, see [26].

The key interest of the more recent LDA+DMFT calculations, which will be discussed in the following, is to shed new light on the actual ground state of  $V_2O_3$  at different points in the phase diagram Fig. 1. Special attention is paid to the insulating and metallic phase of the 1.1% Cr-doped sample in the vicinity of the MIT as well as to the comparison between the metallic phase of the undoped sample at ambient conditions and the Cr-doped sample under external pressure.

In the following, we discuss some aspects and details of the LDA+DMFT calculation in Section 2. Theoretical and experimental results for the optical conductivity are presented in Section 3, those for the photoemission microscopy in Section 4, and those for the X-ray absorption spectroscopy in Section 5. Finally, Section 6 provides a summary and conclusion.

## 2 LDA+DMFT implementation

**2.1 Low energy  $t_{2g}$  NMTO Hamiltonian** The first step of the LDA+DMFT calculations is the derivation of the Hamiltonian for the low-energy  $t_{2g}$  orbitals from the bandstructure calculation via NMTO downfolding or Wannier projections. The Hamiltonian is constructed to capture the relevant degrees of freedom of the system for low energy scales on a reduced basis set. In the case of  $V_2O_3$  we used a model obtained by the NMTO method, with which the full LDA Hamiltonian was downfolded on

the  $t_{2g}$  sub-space around the Fermi energy. As described above (see Fig. 2), the  $t_{2g}$  states are decomposed into a single  $a_{1g}$  and two degenerate  $e_g^\pi$  states. However, if we look closely at the bandstructure in Fig. 3 we find twelve  $t_{2g}$  bands instead of three. The reason for this is simply that there are four vanadium atoms in the primitive unit cell which means, that we obtain a 12 by 12 Hamiltonian as a function of  $\mathbf{k}$  for  $V_2O_3$  from the downfolding. (For a detailed discussion of the downfolding procedure of the  $V_2O_3$  model see Saha–Dasgupta *et al.* [6]). Yet, although the LDA Hamiltonian is a twelve-band dispersion matrix, the actual DMFT calculation can be performed with no more effort than a three band calculation. The reason for this is simply that all four vanadium atoms in the unit cell are located on equivalent sites which means that they are related to one another by symmetry transformations. In other words, each of the four vanadium atoms experiences the same environment and, hence, has the same *local* eigenstates. As a consequence, the  $\mathbf{k}$ -integrated local Green function can be written in a basis in which we obtain four equal diagonal blocks with respect to the site index. The orbital labels  $a_{1g}$  and  $e_g^\pi$  are good quantum numbers *locally*. Such a local basis set is a necessary condition for the formulation of the local interaction parameter  $U$  and a correct definition of the *local* DMFT self energy.

**2.2 DMFT Green function and self energy** We explicitly write the local Green function as:

$$\begin{aligned} \underline{G}^{\text{loc.}}(\omega) &= \frac{1}{V_{\text{BZ}}} \int_{\text{BZ}} d^3k \frac{1}{(\omega + \mu)\underline{1} - \underline{\varepsilon}^{\text{LDA}}(\mathbf{k}) - \underline{\Sigma}(\omega)} \\ &= \begin{pmatrix} \underline{G}^{\text{I}} & & \underline{G}^{\text{hyb.}} \neq \underline{0} \\ & \ddots & \\ \underline{G}^{\text{hyb.}} \neq \underline{0} & & \underline{G}^{\text{IV}} \end{pmatrix} \end{aligned} \quad (1)$$

where the roman numerals serve as a site index, and, as mentioned

$$\underline{G}^i = \begin{pmatrix} G_{a_{1g}}^{\text{loc.}} & 0 & 0 \\ 0 & G_{e_g^\pi}^{\text{loc.}} & 0 \\ 0 & 0 & G_{e_g^\pi}^{\text{loc.}} \end{pmatrix}; \quad \mathbf{i} = \text{I}, \dots, \text{IV} \quad (2)$$

the diagonal blocks are equal for each site  $i$ . Hence, in order to calculate the local DMFT self energy, which clearly has to be the same for all four (locally equivalent) sites, we have to project out only the first diagonal block after the  $\mathbf{k}$ -integration, and proceed with the calculation of the DMFT self energy in the usual way. The resulting self energy is a diagonal 3 by 3 matrix  $\underline{\Sigma}^{\text{I}}(\omega)$  and is used in the next iteration to construct the full 12 by 12 diagonal matrix  $\underline{\Sigma}(\omega)$  taking the equality of the four vanadium sites into account

$$\underline{\Sigma}(\omega) = \begin{pmatrix} \underline{\Sigma}^{\text{I}}(\omega) & 0 & 0 & 0 \\ 0 & \underline{\Sigma}^{\text{I}}(\omega) & 0 & 0 \\ 0 & 0 & \underline{\Sigma}^{\text{I}}(\omega) & 0 \\ 0 & 0 & 0 & \underline{\Sigma}^{\text{I}}(\omega) \end{pmatrix} \quad (3)$$

This full self energy then enters equation (1) for the calculation of the next local Green function. Furthermore, it is important to strongly stress at this point that we do not make additional approximations with the procedure described above. From the DMFT point of view, i.e., the local perspective, the  $V_2O_3$  calculation is de facto just a three orbital problem.

Besides the additional step of projecting out the local part of the full Green function the LDA+DMFT calculation of  $V_2O_3$  is straight forward, see [27,28,29] for more details on LDA+DMFT. Let us now turn to the spectroscopic data and our theoretical interpretation.

**3 Optical conductivity: Phase separation around the MIT** The first work we will discuss, are measurements of infrared optical conductivity [30]. This experiment has a twofold goal: on the one hand, to clarify the behavior of the 1.1% Cr-doped compound around the metal to insulator transition, and on the other hand, to perform an experimental check of the pressure-doping equivalence. The motivation of the former analysis is the following: In the past much effort has been put into the understanding of the transition between the PM and the PI phase Fig. 1. However, somehow less, or at least less concrete, attention was paid to the local strain that occurs in the lattice in the Cr-doped compounds [3,31], even though, for  $(V_{0.989}Cr_{0.011})_2O_3$ , the presence of a structural phase separation, between the PM  $\alpha$ - and PI  $\beta$ -phase, by the Cr-doping has been stated before [3,31,4]. Other experimental studies also support the idea that the Cr- atoms in  $(V_{0.989}Cr_{0.011})_2O_3$  could play the role of  $\beta$ -phase “condensation nuclei”:

Resistivity measurements, for example, show that the conducting phase of weakly Cr-doped samples shows a bad metallic behavior, different from the undoped compound [32]. Moreover, so called extended x-ray absorption fine-structure spectroscopy (EXAFS) measurements showed that the presence of Cr contracts the Cr–V bonds, inducing a concomitant elongation of V–V pair bonds [31]. Such “long” V–V pair bond is associated to the  $\beta$  PI phase [2], as shown also by theoretical calculation using LDA+DMFT [17]. Therefore it may be hypothesized that, within a metallic matrix host, insulating-like “islands” are formed around the Cr impurities [33,34]. On this basis, the PM–PI MIT has been suggested to have also a percolative nature [31]. Pressure-dependent transport studies by Limelette *et al.* [35] were also used to show that across the PI–PM first order transition a large hysteresis occurs. This points to a non-trivial role of the lattice and its distortions due to the Cr doping, which has however been almost disregarded,

or drastically simplified when defining the phase diagram. The latter has been established by means of resistivity data only and suggests the equivalence of doping and pressure.

The relation between such hysteresis and the above mentioned coexistence of  $\alpha$  and  $\beta$ -phases has not been clarified hitherto. It is these unknowns at which the more recent investigation [30] aimed.

**Experimental results** The experimental results [30] are presented in Fig. 4: In the upper panel the positions in the phase diagram where the spectra were taken are marked. The spectra are plotted in the lower panel in the corresponding color: on the left hand side several spectra for different temperatures are shown together with their values for the DC conductivity  $\sigma_{DC}$  at  $\omega \rightarrow 0$ , whereas on the right hand side the  $T=200K$  spectra for the undoped and the 1.1% Cr-doped samples are compared.

Let us start with the discussion of the temperature dependent data. Shown in Fig. 4 (lower panel left hand side) are  $(V_{0.989}Cr_{0.011})_2O_3$ -spectra in the temperature range between 500K and 200K (the sharp peaks around  $500cm^{-1}$  correspond to phonon resonances and are of no further interest for the present discussion). Our starting point is in the cross-over region of the transition at 500K (red). Cooling down we obtain the spectrum at 400K (yellow) and at 300K (green). At 300K, however, we are in the direct vicinity of the transition line. Hence, we can, in fact, find a qualitatively different (PM-phase) spectrum at 300K (light blue) if we approach the same point by heating up from lower temperatures. That is, we observe hysteresis. The last spectrum we show in the plot was taken in the PM phase at 200K (blue). The first three spectra, from 500K down to 300K (upon cooling) display the gapped shape which we expected as the hallmark of the insulating nature of the PI  $\beta$ -phase. The spectra show no Drude peak and, only at elevated temperatures, gain minimal spectral weight at  $\omega \rightarrow 0$ . The remarkable, and far from trivial, spectra are the ones in the PM phase at 300K (upon heating, light blue) and at 200K (blue). We recall that already resistivity measurements have shown a bad metallic behavior for the Cr-doped sample as opposed to the undoped compound. Yet, how dramatic the difference to the undoped sample really is, can be seen clearly in Fig. 4 (lower panel right hand side) where we show a direct comparison of the  $(V_{0.989}Cr_{0.011})_2O_3$ -spectrum at 200K (blue) and the spectrum of the undoped sample at the same temperature (pink): The spectrum of the undoped sample shows the behavior that is expected from a metallic phase, including a well pronounced Drude peak. In contrast, the shape of the spectrum of the Cr-doped compound is rather unexpected: It does not show a Drude peak, but neither has it a gap like in the insulating regime as the spectral weight around  $\omega \rightarrow 0$  is non-negligible. This fact is a clear support for a scenario of an inhomogeneous (i.e.  $\alpha$ - $\beta$  mixed) metallic phase. On the contrary, when comparing the behavior of  $(V_{0.989}Cr_{0.011})_2O_3$  and  $(V_{0.972}Cr_{0.028})_2O_3$  within the PI phase, only small differences appear (not shown here).

These new interesting experimental facts were motivation enough to revisit the compound again with the help of LDA+DMFT in order to understand the features that are displayed more fundamentally. Performing this analysis allows us to test the hypothesis of the mixed  $\alpha$ - $\beta$  phase scenario [30].

**LDA+DMFT analysis** The starting point for the theoretical LDA+DMFT analysis is the downfolded NMTO Hamiltonian described in the previous section for the  $\alpha$ - and the  $\beta$ -phase respectively. In the DMFT code, the Hirsch Fye quantum Monte Carlo method was employed. The calculations were carried out at an inverse temperature of  $\beta = 20 \text{ eV}^{-1} \approx 580K$  and with interaction parameters  $U = 4.0 \text{ eV}$  and  $J = 0.7 \text{ eV}$ . After convergence of the DMFT self consistent loop the single particle Green function on the imaginary time  $\tau$  axis was analytically continued by means of the Maximum Entropy Method [36]. Next, the local self energy was extracted on the real axis in order to calculate the optical conductivity measured in the experiment. In the following we first discuss the direct DMFT results, i.e., spectral functions and local self energy thereby also comparing them to the previous data from Poteryaev *et al.* [19]. Afterwards we present the calculation of the optical conductivity.

**Interaction parameters for  $V_2O_3$**  From the technical perspective, we need to elaborate in more detail on the important issue of choosing the appropriate values for interaction parameters of a specific compound and the theoretical method that is employed.

$V_2O_3$  presents a good example in that respect, since in the literature several different values for  $U$  and  $J$  can be found. The confusion about these parameters partly stems from the improvement in the estimates of their values over the time and partly from the differences in the numerical techniques. A constrained LDA calculation (for the monoclinic antiferromagnetic phase) by I. Solov'yev *et al.* [37] yields the values of  $U = 2.8 \text{ eV}$  and  $J = 0.93 \text{ eV}$  – parameters that later on were employed in some works [38,39,17]. Yet, constrained LDA gives unfortunately only very rough estimates of the values for  $U$ , which not only crucially depend on the electronic structures, but also on the basis set of the model at hand because it is highly sensitive to screening. For example,  $U$  has to be chosen much lower in the case of a LDA+ $U$  calculation (for  $V_2O_3$   $U = 2.8 \text{ eV}$ ) in comparison to DMFT values ( $U \approx 4 \text{ eV}$ ) in order to overcome the deficiency of the static mean field nature of LDA+ $U$  which overestimates ordering and gaps (see e.g. [40]). This leads to the parameter  $U = 4.0 \text{ eV}$  [41] following the philosophy of Held *et al.* [39] and Poteryaev *et al.* [19] that the value of  $U$  should be consistent with the correct physics of  $V_2O_3$ , i.e., the MIT is reproduced within LDA+DMFT. Therefore, it is not surprising that this choice of  $U$  agrees well with the previous LDA+DMFT studies. The result of our analysis clearly demonstrates that the appropriate  $U$  for the LDA+DMFT calculation should be chosen in the range  $4.0 \text{ eV} < U < 4.2 \text{ eV}$  [41], as we

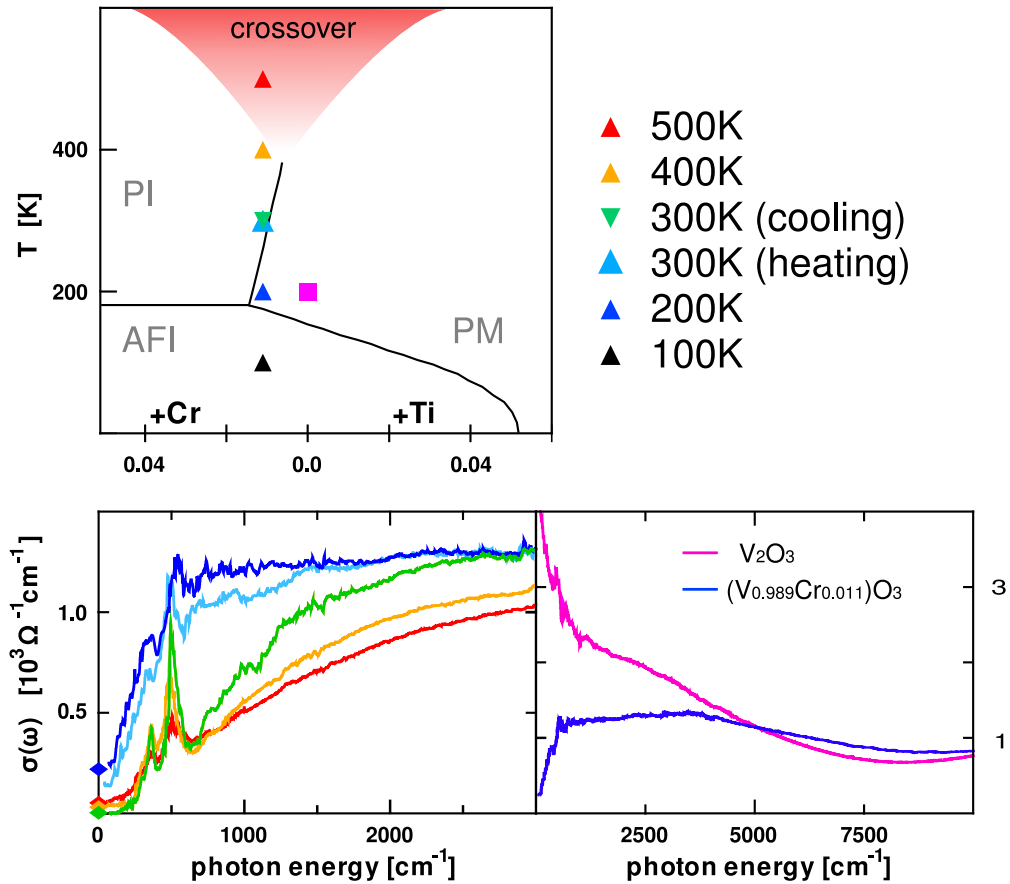


**Figure 4** (Color online) IR optical conductivity for  $V_2O_3$ . Upper panel: phase diagram with marks at the positions where the spectra were taken. Lower panel left hand side: spectra for the 1.1% Cr-doped  $(V_{0.989}Cr_{0.011})_2O_3$  sample at different temperatures ranging from 500K down to 200K. At 300K, hysteresis can be found and the spectra differ severely depending from which phase the point is approached. Lower panel right hand side: comparison between the  $(V_{0.989}Cr_{0.011})_2O_3$  spectrum and the spectrum of undoped  $V_2O_3$  at 220K (according to [30]).

did in the present calculations. Considerably smaller and larger values of  $U$  would either lead to the disappearance or a huge overestimation of the spectral, and as to be seen also optical, gap in the PI phase.

**LDA+DMFT results for  $(V_{0.989}Cr_{0.011})_2O_3$**  In Fig. 5, we report orbital-resolved spectral function (upper panel) as well as the corresponding self energies (lower panels). In the plots we set the Fermi energy to  $\varepsilon_F = 0$  and plot the sum of the two degenerate  $e_g^\pi$  spectra in green, the  $a_{1g}$  spectrum in blue, and the total spectrum, i.e., the sum over all, in red color. We summarize the quantities for the  $\alpha$ - and the  $\beta$ -phase on the left hand and right hand side of the panels respectively. Overall our results agree with the results of the previous LDA+DMFT analysis by Poteryaev *et al.* [19], although we performed the calculations at slightly lower  $U = 4.0$  eV values (in [19]

$U = 4.2$  eV)<sup>2</sup>. The self energies, both real and imaginary parts, display a strongly orbital dependent character. The real part acts like an orbital dependent renormalization of the chemical potential or, in other words, as it is called in Refs. [18,19] as an “effective crystal field” whereas the imaginary part is a measure of lifetime/coherency of the excitations in the associated band. However, the self energy depends also on the filling of the respective orbitals and in a hybridized system like the  $t_{2g}$  states of  $V_2O_3$  it is a very involved quantity: Although the self energy is diagonal we see from equation (1) that its connection to the Green function, and hence the spectrum, involves an inversion so that the orbitally resolved information is, in a way, convoluted.

The spectral functions for the  $\alpha$  and  $\beta$ -phase are quite similar, except for the strongly renormalized coherent quasi-

<sup>2</sup> The reason for our choice is the sensitive dependence of the optical gap on this parameter.

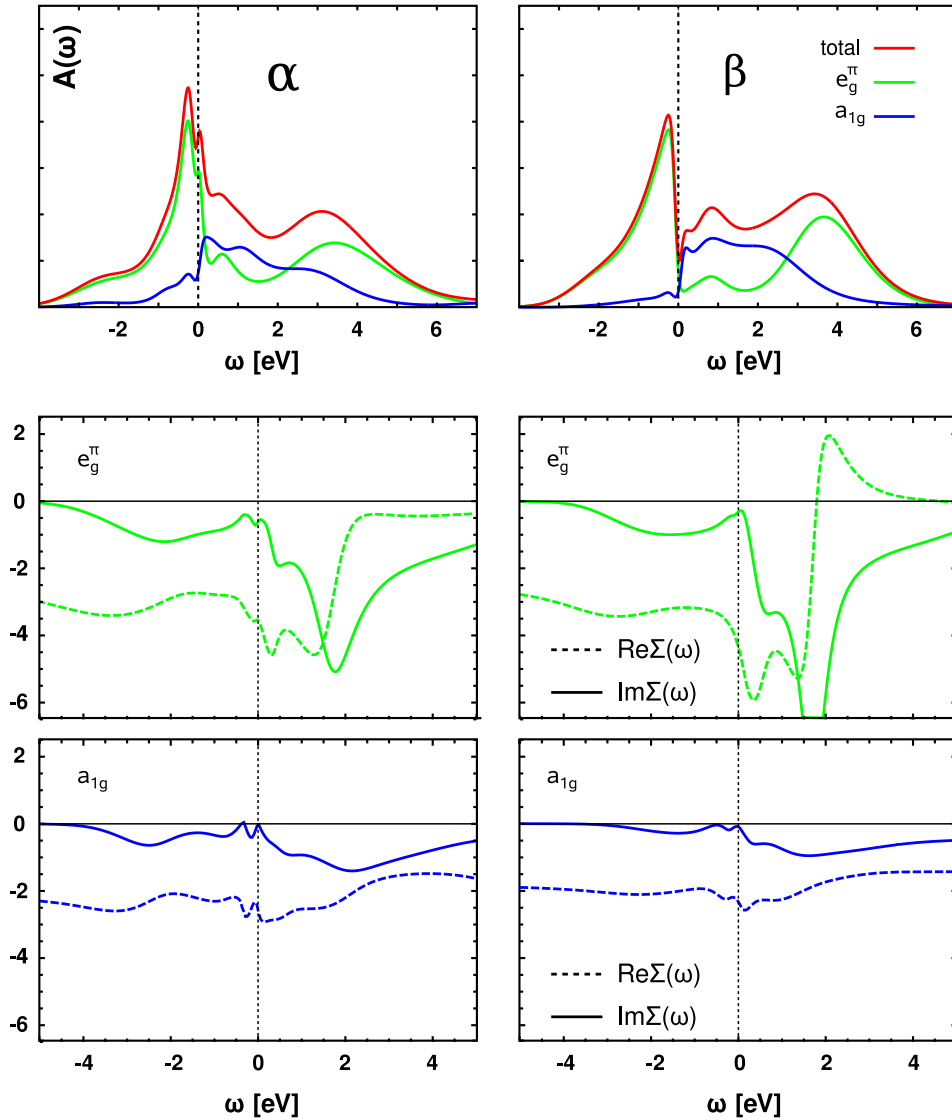


**Figure 5** (Color online) LDA+DMFT results for  $(V_{0.989}Cr_{0.011})_2O_3$  in the  $\alpha$  phase (left hand side) and the  $\beta$  phase (right hand side) for  $U = 4.0$  eV,  $J = 0.7$  eV and inverse temperature  $\beta = 30eV^{-1}$ . In the upper panels we show the LDA+DMFT spectral functions resolved in orbital labels and coded by their color (see legend). The spectra show metallic behavior (coherent excitations around the Fermi energy) for the  $\alpha$  phase and gapped insulating behavior for the  $\beta$  phase. In the lower panels we show the self energies for the  $e_g^\pi$  (middle) and  $a_{1g}$  (bottom) states.

particle excitations of the correlated metallic  $\alpha$ -phase around the Fermi energy. Of course, the differences are expected to be sharpened up at lower temperatures. From the orbital-resolved spectra we can obtain valuable insight. Let us have a closer look at the incoherent part of the spectrum, i.e., the Hubbard bands. The basic features can be understood as follows: As it was discussed in previous works (e.g. [39]) and also will be confirmed later by the XAS study [42] the predominant local configuration on the V atoms has two spin-aligned electrons in the  $e_g^\pi$  orbitals, i.e., a  $|e_g^\pi e_g^\pi\rangle$  spin-1 configuration, with some

admixture of  $|a_{1g}e_g^\pi\rangle$  spin-1 configurations. For a simple picture let us first consider the lower Hubbard band (LHB), that is, the electron removal part of the spectrum. We recall the relevant onsite interaction parameters to be the intra-orbital interaction  $U$ , the inter-orbital interaction  $V$ , and the spin-coupling constant  $J$ . Furthermore, in cubic (or close to cubic) symmetry the relation  $V = U - 2J$  holds. Starting either from the  $|e_g^\pi e_g^\pi\rangle$  or the  $|a_{1g}e_g^\pi\rangle$  configuration, the removal of an electron will result in an energy gain of  $V - J$  ( $\approx 1.9$  eV in our case) which is in agreement with the position of the LHB. The only structure, i.e.



splitting, which occurs is the crystal field potential differences of the  $e_g^\pi$  and  $a_{1g}$  states. This energy scale, however, is below the resolution of our spectra at high  $|\omega|$ . For the upper Hubbard band, i.e., the electron addition part, the situation turns out to be a little bit different. The additional electron can either populate an  $e_g^\pi$  or an  $a_{1g}$  state. Then the process  $|e_g^\pi e_g^\pi\rangle \rightarrow |e_g^\pi e_g^\pi e_g^\pi\rangle$  or  $|a_{1g} e_g^\pi\rangle \rightarrow |a_{1g} a_{1g} e_g^\pi\rangle$  will cost an energy of  $U + V$ . The additional electron interacts via  $U$  with one of the other two electrons, and via  $V$  with the other one. Transitions  $|e_g^\pi e_g^\pi\rangle \rightarrow |e_g^\pi e_g^\pi a_{1g}\rangle$  or  $|a_{1g} e_g^\pi\rangle \rightarrow |e_g^\pi e_g^\pi a_{1g}\rangle$  only cost  $2V$  or  $2V - 2J$  depending on the respective spin alignment. Consequently, the UHB is split into two main features which we can find around 1 eV and 4 – 5 eV. We conclude that i) the split of the UHB depends apparently strongly on the choice of  $J$  and ii) this splitting is responsible for the small width of the gap compared to the interaction parameters<sup>3</sup>.

Let us, finally, turn to the optical conductivity. The LDA+DMFT calculation of the optical conductivity has been performed within the Peierls approximation and neglecting vertex corrections along the line of [23].<sup>4</sup>

In Fig. 6 we show a comparison of experimental data (left hand side) and LDA+DMFT data (right hand side). We calculated the optical conductivity also for both  $\alpha$  and  $\beta$ -phase. The LDA+DMFT optical conductivity of the  $\beta$ -phase (right hand side: blue) shows a gapped behavior, as it is expected for the PI phase. The fact that it does not extrapolate to zero at energies lower than  $1000\text{cm}^{-1}$  is due to the temperature of  $\beta^{-1} = 0.05\text{eV} \approx 500\text{K}$  assumed for the DMFT(QMC) calculations. Further, when we compare it to the experimental data of the 2.8% Cr-doped sample, deep in the PI phase, we see that the calculated gap of [30]  $\sigma_\beta$  is a little bit too large. The reason for this overestimation is an extreme sensitivity of the calculation on the choice of  $U$  and  $J$  as it was already mentioned before<sup>5</sup>. The calculated  $\alpha$ -phase optical conductivity (right hand side: red) shows an overall good agreement with the experimental data taken for the undoped compound (left hand side: red). At  $\omega \rightarrow 0$  we can distinguish the typical Drude peak contribution of the PM phase.

The most interesting spectrum, however, corresponds to the experimental data taken for the 1.1%Cr-doped sample at 200K (left hand side: green): As mentioned above this spectrum is strange in its shape (with neither Drude

peak nor gap) and belongs to a state that is, according to the resistivity measurements, a bad metal. The discrepancy between the idea that the PM phase can be seen as a uniform metallic phase and the experimental evidence is further enhanced by our LDA+DMFT calculations. Specifically, as the lattice parameters practically do not change within the  $\alpha$ -phase, the LDA+DMFT spectrum of the 1.1%Cr-doped sample at 200K and of the undoped compound are basically indistinguishable. Hence, our calculations support the hypothesis of an  $\alpha$ - $\beta$  phase mixture in the bad metal region. To test this hypothesis further we resort to a semi-empirical formula of the *effective medium theory* (EMT) [33,44] which provides a simple way of approximating the dielectric constants  $\bar{\varepsilon}(\omega) = (1 + 4\pi i\sigma(\omega)/\omega)$  for mixtures of insulating and metallic phases. Within the EMT the effective constant  $\bar{\varepsilon}(\omega)_{\text{eff}}$  satisfies the condition

$$f \frac{\bar{\varepsilon}_{\text{met.}}(\omega) - \bar{\varepsilon}_{\text{eff.}}(\omega)}{\bar{\varepsilon}_{\text{met.}}(\omega) + \frac{1-q}{q}\bar{\varepsilon}_{\text{eff.}}(\omega)} + (1-f) \frac{\bar{\varepsilon}_{\text{ins.}}(\omega) - \bar{\varepsilon}_{\text{eff.}}(\omega)}{\bar{\varepsilon}_{\text{ins.}}(\omega) + \frac{1-q}{q}\bar{\varepsilon}_{\text{eff.}}(\omega)} = 0 \quad (4)$$

Where  $f$  and  $q$  are free fitting parameters which are phenomenologically related to the size and relative densities of the “islands” of the two constituent phases. For further information about this approach we refer the reader to [45]. Now we take the optical conductivity spectra measured in the undoped sample and the 2.8% Cr-doped sample as the  $\alpha$ - and  $\beta$ -phase spectra respectively and use Eq. (4) to fit the experimental spectra of the 1.1% Cr-doped sample. For the values  $f = 0.42$  and  $q = 0.35$  an excellent agreement can be found which is plotted in Fig. 6 (left hand side: compare green and gray). From a theoretical point of view, it is even possible to directly use the LDA+DMFT spectra for the  $\alpha$ - and  $\beta$ -phase of  $(\text{V}_{0.989}\text{Cr}_{0.011})_2\text{O}_3$  as an input for the EMT. Also in this case, with the same values of  $f$  and  $q$  we obtain a satisfying agreement with the experimental data.

To sum up, the experimental measurements of the optical conductivity together with the theoretical interpretation by means of LDA+DMFT strongly support the scenario of a mixed phase state for the 1.1% Cr-doped compound at 200K. It will be seen in Section 5 that the complementary x-ray absorption spectroscopy also speaks for this scenario.

The last part of our discussion about the optical conductivity is devoted to the data of the 1.1% Cr doped sample under pressure far in the metallic region at 6kbar. As it was stated in the beginning, and motivated by the results we already discussed, the second question we want to address is whether the doping with Cr can really be “reversed” by applying an external pressure. In short: Can pressure really be drawn on the same axis in the phase diagram as the doping? Experimental results from optical spectroscopy give a clear negative answer to that question. In Fig. 7 we report on the left hand side the comparison of the experimentally measured spectra for the undoped and the 1.1% Cr-doped sample [30]. The spectra are, evidently,

<sup>3</sup> This observation explains also why the attempt to handle the gap (actually the optical gap) with a one band Hubbard model [43] led to unphysically small values for the interaction parameter.

<sup>4</sup> It should be remarked, that the non-monoatomic basis of the crystal leads to corrections in the calculation of the Fermi velocities even at the level of the Peierls approximation as it is discussed by Tomczak [23] and Tomczak and Biermann [24]. For  $\text{V}_2\text{O}_3$ , however, such corrections only concern the optical conductivity along the  $c$  axis not in the  $xy$ -plane.

<sup>5</sup> A slightly larger  $U$ , like it was used, e.g., in [19] would result in an even larger gap.

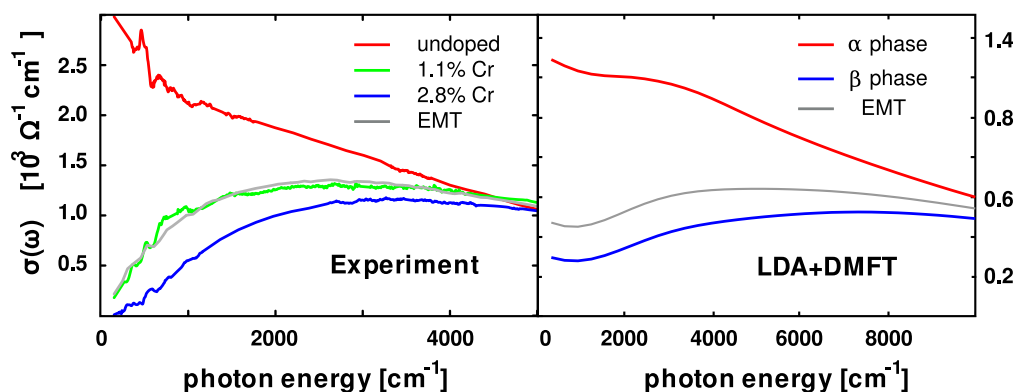


**Figure 6** (Color online) Phase mixing: Comparison of experimentally observed (left hand side) and LDA+DMFT calculated (right hand side) optical conductivity. In red we plot the spectrum for the  $\alpha$  phase, for which we take the experimental spectrum of the undoped sample [30]. The  $\beta$  phase, for which we take the experimental spectrum of the 2.8% Cr doped sample is shown in blue. The measured spectrum of the 1.1% Cr doped sample (green) can be fitted by a mixture of  $\alpha$  and  $\beta$  phase spectra (grey) within the *effective medium theory* [30].

not even qualitatively similar. This indicates the existence of different PM states obtained by either tuning temperature/doping or applying pressure.

It remains, however, to formulate and quantify this difference in a rigorous manner. This will be the subject of the section 5, in which we discuss the hard x-ray absorption spectra on the vanadium K-edge.

**4 Photoemission microscopy** Recently, also spatially resolved photoemission microscopy data was obtained for the 1.1% Cr-doped compound [30]. This experimental technique makes it possible to obtain the detailed physical information of photoelectron spectroscopy with a lateral resolution of the order of 100 nm [46], and has already proven its capability of spatially resolving inhomogeneous electronic structures [47] that would otherwise give an average signal with macroscopic probes [48]. Applied to the 1.1% Cr-doped compound, this method provides a spectacular confirmation of our interpretation based on a mixed phase state in the paramagnetic metallic phase: in Fig. 8 we show the microscopic images together with the PES for the labeled positions. At 260K one clearly observes a mixture of areas with coherent excitations (with finite spectral weight at the Fermi energy) and insulating regions (gapped spectra) as we would expect in our scenario. Upon heating, the system becomes completely insulating (compare the image at 320K). Note, after cooling down to 220K again the same “map” as before is recovered. Note, differences in Fig. 8 between 220 and 260K are due to the different temperatures, not due to the hysteresis loop, see the additional data in [30]. This memory effect becomes even more evident in a similar study on the phase transition between the paramagnetic metallic and the antiferromagnetic insulating phase [49]. This suggests a correlation between the position of the insulating

regions and the nucleating action of structural defects in the material, which tend to guide the natural tendency of this system towards phase separation. The structural defects may well be related to the lattice strain caused by the presence of Cr-impurities in the material, even though this conjecture has to be further clarified both experimentally and theoretically.

#### 5 X-ray absorption on the V-K-edge: Pressure vs. doping

Among the different experimental methods recently employed to study the electronic properties of the Mott transition in Cr-doped  $V_2O_3$  [35,50,51,42,52], X-ray absorption spectroscopy (XAS) has played a crucial role. For instance, it was the detailed investigation of the V  $L_{2,3}$  absorption edges [5] that demonstrated the necessity of abandoning the simple one band,  $S = 1/2$ , model to obtain a realistic description of the changes in the electronic structure at the phase transition. Further, Park *et al.* obtained valuable quantitative information about the vanadium ground state for different amounts of doping and temperatures [5] and formulated it as a linear combination of the  $|e_g^\pi e_g^\pi\rangle$  and the  $|a_{1g} e_g^\pi\rangle$  states which were mentioned earlier. This kind of tool would be perfect to also clarify the question which remains from the discussion of the previous section: What is the character of the metallic ground state of the Cr-doped sample under pressure? However, unfortunately the V  $L_{2,3}$  absorption falls in the region of soft x-ray radiation, and thus, due to the specific absorption characteristic of the diamond anvil cell used for the pressure measurements, it cannot be employed in our case. But fortunately XAS can also be performed at the V K-edge in the hard x-ray range, i.e., in a spectral region without particular absorption of the diamond anvil cell. In this case, the pre-edge will carry most of the physical information

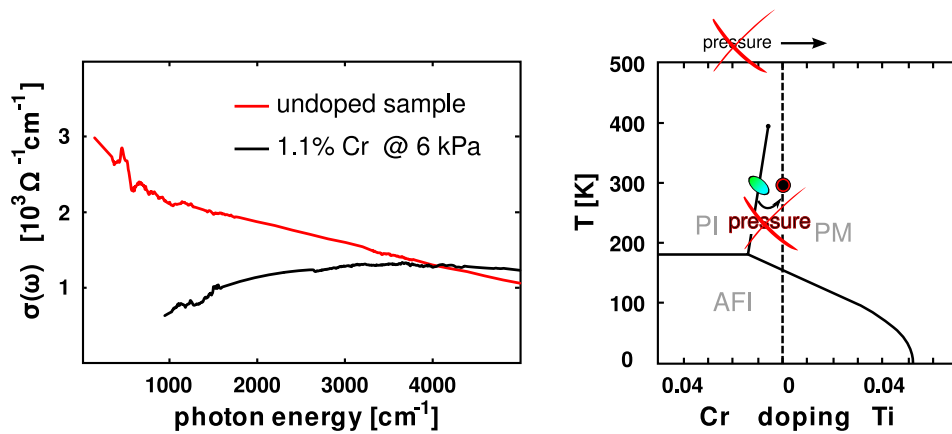


**Figure 7** (Color online) Left: Experimental measurements of the optical conductivity for the undoped sample (red) and the 1.1% Cr doped sample at 6 kbar [30]. For this pressure the “common wisdom” of a pressure-doping equivalence would predict a fully recovered PM phase equivalent to the undoped compound PM phase. Right: The experimental data clearly proves this assumption to be incorrect and suggests to abandon the concept of pressure equals inverse doping.

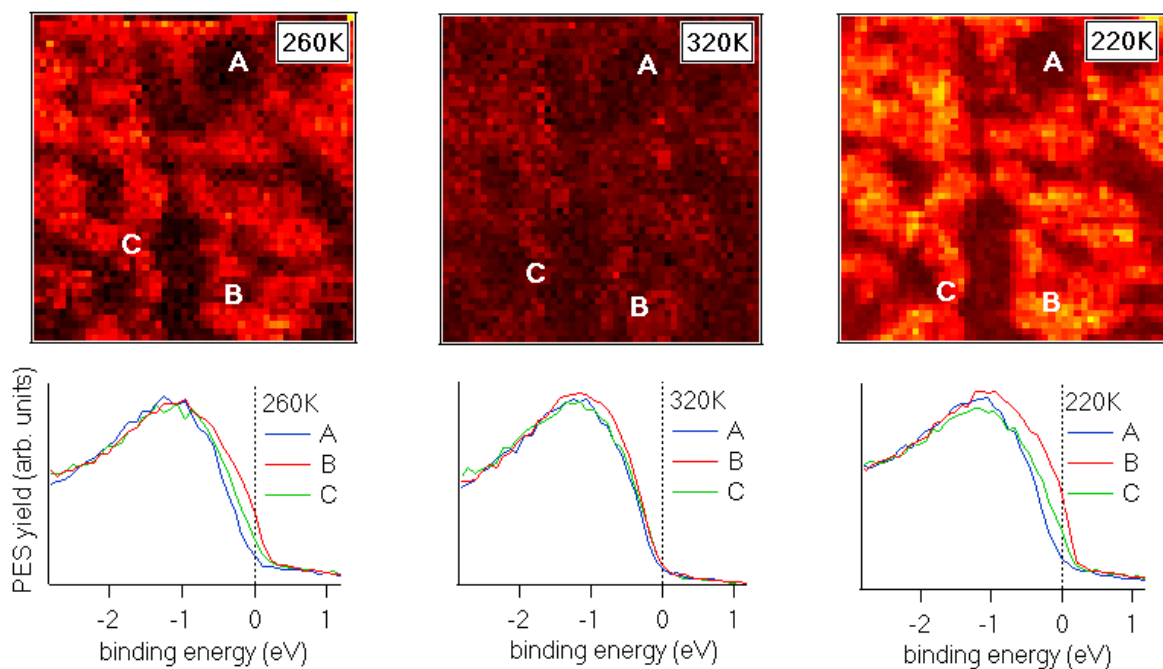


**Figure 8** (Color online) Representative intensity ratio images and corresponding photoemission spectra at different temperatures over a  $50 \mu\text{m}$  by  $50 \mu\text{m}$  area obtained by scanning photoemission microscopy using photons at 27 eV [30]. Inhomogeneous properties are found within the PM phase at 220 or 260 K, where metallic (bright) and insulating (dark) domains coexist. A homogeneous insulating state is instead obtained in the PI phase at 320 K. After a whole thermal cycle the structure of the inhomogeneous distribution is recovered, indicating the presence of stable “condensation nuclei”.

we are interested in, as it is predominantly due to  $1s \rightarrow 3d$  transitions. The excitations in this pre-edge region are influenced also by the core hole and should be considered to be of an excitonic nature. Beside the possibility of measuring the V  $K$ -edge under pressure condition we obtain also a more straightforward interpretation. Namely, due to the simple spherical symmetry of the  $s$ -core hole, the multiplet structure reveals a more direct view on the  $d$ -states. Motivated by the above considerations, we used in Ref. [42,53] V  $K$ -edge XAS to explore extensively the MIT in  $V_2O_3$  by changing temperature, doping and applying an external pressure. The onsets of the  $K$ -edges were analyzed by a novel computational scheme combining the LDA+DMFT method with configuration interaction (CI) full multiplet ligand field calculations to interpret subtle differences at the PM-PI transition.

Such CI, or as they are frequently called 'cluster calculations' became within the last 25 years a popular parameter based method for fitting experimental data in order to extract information on charge, spin, and orbital degrees of freedom particularly in correlated transition metal oxides (see e.g. Refs. [54,55,56,57]). In this work, however, we do not fit to experiment, but instead use parameters derived from an *ab initio* LDA+DMFT scheme in order to calculate the experimentally measured x-ray spectrum (for further, more technical details see Ref. [7]).

This analysis allowed us to: (i) observe in detail the changes in the electronic excitations, providing also a direct estimate of the Hund's coupling  $J$  (recall the discussion of the LDA+DMFT spectral functions in the previous chapter) (ii) analyze the physical properties of the PI and PM phase on both sides of the MIT, leading to the main result of our work: (iii) understand the difference between P, T or doping-induced transitions. This difference is mainly related to the occupancy of the  $a_{1g}$  orbitals, suggesting the existence of a new "pressure" path between PI and PM in the phase diagram, which is distinctive from the "doping" path. The XAS is in that respect complementary to the optical conductivity measurements. The optical conductivity is connected to somewhat non-local excitations. Therefore it was a great tool to confirm the mixed phase scenario. In contrast the XAS, or more specifically the excitonic features of XAS offers us information about the  $d$  occupations from a completely localized perspective which is needed in order to formulate the ground state in the language of localized Wannier orbitals. This information in turn could not be extracted from the optical conductivity.

For the experiments high quality samples of  $(V_{1-x}Cr_x)_2O_3$  with various doping in the PM ( $x = 0$ ) and PI phases ( $x = 0.011$  and  $0.028$ ) at ambient conditions were used in [42]. The MIT was also crossed for the 0.011 doping by changing temperature and for the 0.028 doping by pressure. To obtain the best resolution, the XAS spectra were acquired in the so-called partial fluorescence yield (PFY) mode [58], monitoring the intensity of the V- $K\alpha$

( $2p \rightarrow 1s$ ) line as the incident energy is swept across the absorption edge. Further experimental details can be found in [42,53].

**Powder data and isotropic calculations** The T-dependent absorption spectra are displayed in Fig. 9 left hand side for both PM (200 K) and PI (300 K) phases for the  $x = 0.011$  powder sample. The spectra have been normalized to an edge jump of unity. We will focus on the pre-edge region, where information about the V  $d$ -states can be extracted as it is indicated in the plot. It can be decomposed into three spectral features (A,B,C) which all vary in intensity as the system is driven through the MIT whereas C is considerably broader than A and B. Notice that no feature is observed below peak A contrary to the early results of Ref. [59] but in agreement with the more recent data of Ref. [60]. Within a simplified atomic like picture, one could directly relate the intensity of features A,B and C to the unoccupied states: The  $V-t_{2g}^2$  states are split into one  $a_{1g}$  and two  $e_g^\pi$  states under trigonal distortion of the V sites [6] as shown in Fig. 2. Starting from a  $V-t_{2g}^2$ ,  $S = 1$  configuration, one can either add an electron to the  $t_{2g}$  subshell yielding peaks A and B, or add an electron to the  $e_g^\sigma$  sub-shell which gives rise to the broader peak C. In this picture, Hund's rule exchange splits peaks A and B into a quartet ( $S = 3/2$ ) and doublet ( $S = 1/2$ ) states.

This point of view is, however, oversimplified as the V  $d$  electrons are *strongly correlated* and, in the pre-edge region, the spectra are still largely influenced by the  $1s$  core hole potential. Keeping that in mind, we have simulated in [42,7] the pre-edge by combining CI with LDA+DMFT calculations for which the one particle part (LDA) input corresponds to the level diagram in Fig. 2. We concentrate our analysis to peaks A and B, since peak C relates mainly to the unoccupied  $e_g^\sigma$  orbitals. These hybridize much stronger with the ligands and thus lack direct information on the Mott transition; peak C may also be related to non-local excitations (not included here) [61] which sensitively depend on the metal-ligand distance. Let us also note that the V sites in  $V_2O_3$  are non centro-symmetric which leads to an on-site mixing of V- $3d$  and V- $4p$ -orbitals and interference between dipole and quadrupole transitions [62]. This interference has been included in our scheme, see [7] for details, together with the linear dichroism measurements.

The CI calculations [42,7] confirm that for the ground state the occupancy ratio between the ( $e_g^\pi, a_{1g}$ ) and ( $e_g^\pi, e_g^\pi$ ) states is smaller in the PI than in the PM phase [18,5]: The isotropic CI-based calculated XAS spectra in the pre-edge region reported in Fig. 9 right hand side agree well with the experimental data for both the energy splitting of features A and B and the ratio of their spectral weight (SW) which increases in the PM phase.

Considerable insight can be gained by comparing CI and LDA+DMFT calculations. Our LDA+DMFT calculations [42], performed using the same NMTO Hamiltonian

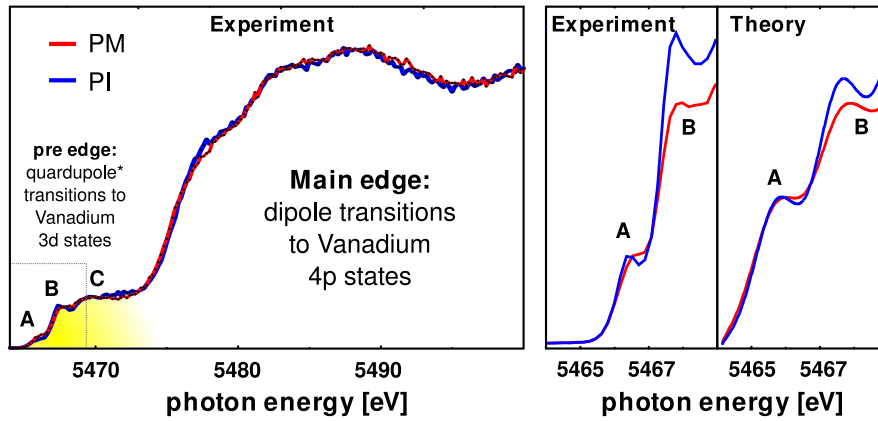


**Figure 9** (Color online) Vanadium  $K$ -edge x-ray absorption spectra in  $(V_{1-x}Cr_x)_2O_3$  for a powder sample with  $x = 0.011$  measured as a function of temperature ( $T$ ) in the PM (200 K, red line) and PI (300 K, blue line) phase by partial fluorescence yield XAS. In the region above 5475 eV the main edge starts; here dipole transitions from the core electron to the vanadium 4p states give the main contribution. Below 5470 eV we find the pre-edge – where, besides others, the transitions to the vanadium 3d states are located. From these we extract the information about the ground state of the system. On the right hand side we show a zoom of the pre-edge region and compare the structure to theoretical full multiplet CI spectra. As explained in the text, these transitions would be pure quadrupole if it would not be for the inversion symmetry breaking on the vanadium site that makes the transitions “slightly dipole allowed”. (reprinted with permission from [42] Copyright (2010) by the American Physical Society))

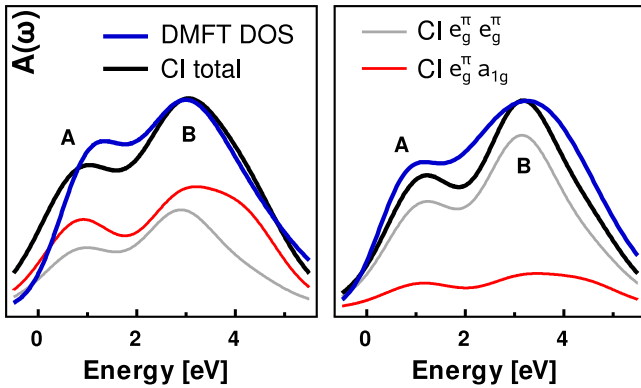


**Figure 10** (Color online) Spectral function  $A(\omega)$  comparing “incoherent” LDA+DMFT part (blue line) and the CI calculation (black line) in the pre-edge region; left panel: PM, right panel: PI phase;  $\varepsilon_F = 0$  is the Fermi energy. Note the similarity in the main spectral features when crossing the MIT. Also shown are the different contributions of the CI spectrum labeled accordingly to their initial state: the contribution of the  $(e_g^\pi, a_{1g}) \rightarrow (e_g^\pi, e_g^\pi, a_{1g})$  transitions (red line) to the peak A(B) is approximately 60%(55%) in the PM phase and 20%(15%) in the PI phase (reprinted with permission from [42] Copyright (2010) by the American Physical Society).

with the 1.1% Cr-doped  $V_2O_3$  and Hirsch–Fye Quantum Monte Carlo as impurity solver, confirm the above mentioned tendency. Specifically we obtain a mixing of 50:50 and 35:65 for the  $(e_g^\pi, a_{1g}) : (e_g^\pi, e_g^\pi)$  occupation in the PM and PI phases respectively. Remarkably the simple structure of the core hole potential in the  $K$ -edge spectroscopy ( $L = 0$  i.e. spherical potential) allows us to associate the pre-edge spectrum with the  $k$ -integrated spectral function above the Fermi energy calculated by LDA+DMFT in which we do not take into account the core hole effects. The electron-addition part of the spectral function shows three main features in PM phase: a coherent excitation at the Fermi level and a much broader double peak associated to the incoherent electronic excitations, i.e., the upper Hubbard band (UHB), almost identically to the undoped compound. In the PI phase obviously, only the latter survives. Comparison with the experimental spectra clearly shows that the pre-edge features have to be related to the “incoherent” part of the spectral function only. The physical reason is that the core hole potential localizes the electrons destroying the (already strongly renormalized) coherent quasiparticle excitations and making the XAS spectrum atomic-like. The “incoherent” LDA+DMFT, CI and experimental spectra shown in Figs. 10 and 9, respectively, agree in many aspects, especially as for the splitting of the first two peaks by  $\approx 2.0$  eV ( $\approx 1.8$  eV in experiment) which originates in LDA+DMFT from the Hund’s exchange  $J$  in the Kanamori Hamiltonian (see discussion of the LDA+DMFT spectral functions in Section 3). This further validates the choice of  $J = 0.7$  eV used in our

calculations in contrast to larger values assumed in previous studies [18,63], and also clarifies the mismatch between XAS and LDA+DMFT spectra reported in the undoped  $V_2O_3$  compound [18] where incoherent excitonic features were identified by coherent quasiparticle excitations. Moreover, the ratio between A and B peak displays the same trend in the PM-PI transition as the CI (or experimental) data. The quantitative difference between the two calculations is attributed to the lack of matrix elements in LDA+DMFT.

The intensity ratio of the first two incoherent excitations peaks A and B (associated to the quartet and doublet states in the oversimplified picture) thus appears as the key spectral parameter to understand the differences between PM and PI. Even in a powder sample, this ratio is still sensitive to the  $a_{1g}$  orbital occupation of the initial state. Indeed, due to the trigonal distortion a considerable spectral weight transfer from the peak B to higher energies (corresponding to final states with two  $a_{1g}$  electrons) can take place for the  $(e_g^\pi, a_{1g})$  but not for the  $(e_g^\pi, e_g^\pi)$  initial state. Therefore, the  $K$  pre-edge XAS can serve as a direct probe of the  $a_{1g}$  orbital occupation in the ground-state. As a rule of thumb, the larger the ratio between the SW of A and B, the larger the  $a_{1g}$  orbital occupation.

**Under pressure** After we established an interpretation scheme of the vanadium XAS  $K$ -edge which allows us to use it as a ground state occupation probe it is time to come back to the original task of inquiring the metallic phase of Cr-doped  $V_2O_3$ . Fig. 11 shows the XAS powder spectra of the pressure-induced MIT with the corresponding spectra for the temperature- and doping-driven transition (the markers in the phase diagram, Fig. 11). We remark at this point that the spectra taken under pressure display a relative shift between main-edge (not shown) and pre-edge, which is in any case irrelevant for our discussion of the ground state for which we only need the intrinsic structure of the pre-edge. Hence, this shift is compensated for the pressure spectra in Fig. 11. Fig. 11 clearly evidences that (besides the shift) contrary to the doping- or T-driven transition, very small changes in spectral shapes and weights are observed in the pressure driven MIT. In the light of the arguments discussed above, our finding proves that the metallic state reached by applying pressure is characterized by a much lower occupation of the  $a_{1g}$  orbitals compared to the metallic state reached just by changing temperature or doping. Importantly, the spectra measured through the doping induced MIT are identical within the experimental uncertainty to those measured through the temperature driven transition. The temperature-doping equivalence is confirmed by photoemission data [64] and is consistent with the very similar lattice parameter changes across the transition [2]. The  $x$  and  $T$  equivalence is also borne out by the observation from XAS at the  $L$ -edges in doped  $V_2O_3$  [5] that the  $a_{1g}$  occupation within both the PM or PI phases is mostly independent of the doping level. Hence, the local incoherent excitations probed by XAS at the V

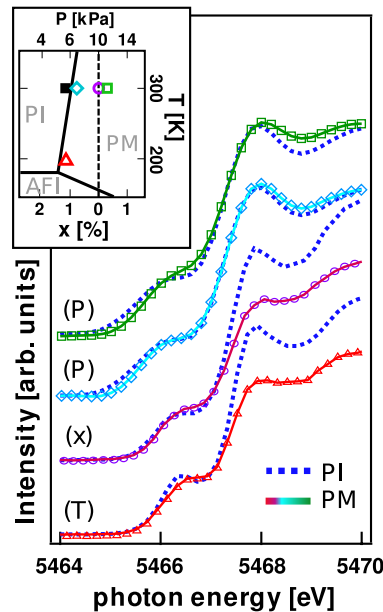


**Figure 11** (Color online) V–K edge XAS spectra for powder samples of  $(V_{1-x}Cr_x)_2O_3$ , starting from the top, as a function of pressure (P) ( $\square$ ) [ $x = 0.028$ ; 5 and 11 kbar (topmost set of curves); 5 and 7 kbar (second highest set of curves)], temperature ( $\triangle$ ) [ $x = 0.011$ ; 200,300 K (second lowest set of curves)] (T), and doping ( $\circ$ ) [ $x = 0, 0.011$  (bottom curves)] ( $x$ ) (cf. points in the phase diagram; the pressure scale refers to the  $x = 0.028$  doping). The spectral differences demonstrate the nonequivalence between  $P$  and temperature-doping. The  $x$ - $T$  equivalence is confirmed by the photoemission spectra [64].

$L$  edge or  $K$  pre-edge are not directly affected by disorder [31]. The reason for this is that XAS is a *local probe* in the sense that we can expect the changes in the XAS spectrum to be of the order of the percentage of the atoms which have a different ground state.

**6 Conclusion** The presented findings clearly shows the limits of the common assumption that temperature, doping, and pressure-driven MITs in  $V_2O_3$  can be equivalently described within the same phase diagram<sup>6</sup> [2]. Indeed, the two different PM electronic structures that we observed reflect different mechanisms driving the MIT along different pathways. In the doping-driven MIT, the metallic phase is characterized by an increased occupation of the  $a_{1g}$  orbitals indicating a reduced “effective crystal-field-splitting” as the main driving mechanism towards metallicity [18,19], related to the jump of the lattice parameter  $c/a$  (1.4%) at the MIT [2]. In contrast, when pressure is

<sup>6</sup> An early version of the phase diagram (Fig.15 in [2]) was actually drawn with a third pressure axis, but due to the idea of  $p$ - $x$  equivalence, this was later abandoned.



applied, the  $a_{1g}$  occupation remains basically unchanged, so that this metallic phase seems to originate rather from an increased bandwidth, without any relevant changes of the orbital splitting. The smaller  $c/a$  jump observed under pressure (0.7 %) corroborates our analysis.

Doping, temperature and pressure are shown to act differently on the interplay between electron correlations and crystal field, so that states previously considered to be equivalent metals are actually different.

A second important recent finding is the phase separation within the “paramagnetic metallic” phase for slightly Cr-doped  $V_2O_3$ . Photoemission microscopy clearly reveals this phase separation on the microscale, showing that the “paramagnetic metallic” phase is actually a mixture of metallic and insulating regions. This requires the electrons to percolate inbetween the insulating regions, and hence leads to a reduced conductivity. In the optical conductivity this is reflected by a pronounced dip at low frequencies. This optical conductivity dip of phase-separated  $(Cr_{0.011}V_{0.989})_2O_3$  can be well described within the effective medium theory, either based on the experimental or on the LDA+DMFT optical conductivities (insulating plus metallic phase).

**Acknowledgement** We thank O. K. Andersen, M. Capone, M. Haverkort, N. Parragh and P. Wissgott for valuable discussions regarding the theory. The experimental results described in this paper have been obtained thanks to the collaborative effort of many colleagues, in particular B. Mansart, L. Baldassarre, F. Rodolakis, E. Papalazarou, A. Perucchi, D. Nicoletti, J.-P. Rueff, A. Barinov, P. Dudin and L. Petaccia. We acknowledge financial support from DFG Research Unit FOR 1346 project ID I597-N16 of the Austrian Science Fund (FWF), the EU-Indian network MONAMI, and the RTRA Triangle de la Physique. The calculations for the results presented have been done in part on the Vienna Scientific Cluster (VSC).

## References

- [1] D. B. McWhan, A. Menth, J. P. Remeika, W. F. Brinkman, and T. M. Rice, *Phys. Rev. B* **7**, 1920–1931 (1973).
- [2] D. B. McWhan and J. P. Remeika, *Phys. Rev. B* **2**, 3734–3750 (1970).
- [3] D. B. McWhan, T. M. Rice, and J. P. Remeika, *Phys. Rev. Lett.* **23**, 1384–1387 (1969).
- [4] W. R. Robinson, *Acta Crystallographica Section B* **31**, 1153–1160 (1975).
- [5] J. H. Park, L. H. Tjeng, A. Tanaka, J. W. Allen, C. T. Chen, P. Metcalf, J. M. Honig, F. M. F. de Groot, and G. A. Sawatzky, *Phys. Rev. B* **61**, 11506–11509 (2000).
- [6] T. Saha-Dasgupta, O. K. Andersen, J. Nuss, A. I. Poteryaev, A. Georges, and A. I. Lichtenstein, *arXiv.org* **0**, 0907.2841 (2009).
- [7] P. Hansmann, M. W. Haverkort, A. Toschi, G. Sangiovanni, F. Rodolakis, J. P. Rueff, M. Marsi, and K. Held, *Phys. Rev. B* **85**, 115136 (2012).
- [8] C. Castellani, C. R. Natoli, and J. Ranninger, *Phys. Rev. B* **18**, 4945–4966 (1978).
- [9] C. Castellani, C. R. Natoli, and J. Ranninger, *Phys. Rev. B* **18**, 4967–5000 (1978).
- [10] C. Castellani, C. R. Natoli, and J. Ranninger, *Phys. Rev. B* **18**, 5001–5013 (1978).
- [11] R. M. Moon, *Phys. Rev. Lett.* **25**, 527–529 (1970).
- [12] L. Paolasini, C. Vettier, F. de Bergevin, F. Yakhov, D. Manix, A. Stunault, W. Neubeck, M. Altarelli, M. Fabrizio, P. A. Metcalf, and J. M. Honig, *Phys. Rev. Lett.* **82**, 4719–4722 (1999).
- [13] S. Di Matteo, N. B. Perkins, and C. R. Natoli, *Phys. Rev. B* **65**, 054413 (2002).
- [14] L. F. Mattheiss, *Journal of Physics: Condensed Matter* **6**, 6477–6484 (1994).
- [15] I. S. Elfimov, T. Saha-Dasgupta, and M. A. Korotin, *Phys. Rev. B* **68**, 113105 (2003).
- [16] A. Georges, G. Kotliar, W. Krauth, and M. J. Rozenberg, *Rev. Mod. Phys.* **68**, 13 (1996).
- [17] K. Held, G. Keller, V. Eyert, D. Vollhardt, and V. I. Anisimov, *Phys. Rev. Lett.* **86**, 5345–5348 (2001).
- [18] G. Keller, K. Held, V. Eyert, D. Vollhardt, and V. I. Anisimov, *Phys. Rev. B* **70**, 205116 (2004).
- [19] A. I. Poteryaev, J. M. Tomczak, S. Biermann, A. Georges, A. I. Lichtenstein, A. N. Rubtsov, T. Saha-Dasgupta, and O. K. Andersen, *Physical Review B (Condensed Matter and Materials Physics)* **76**, 085127 (2007).
- [20] M. Schramme, PhD thesis, Universität Augsburg, 2000.
- [21] S. K. Mo, J. D. Denlinger, H. D. Kim, J. H. Park, J. W. Allen, A. Sekiyama, A. Yamasaki, K. Kadono, S. Suga, Y. Saitoh, T. Muro, P. Metcalf, G. Keller, V. Held, K. Eyert, V. I. Anisimov, and D. Vollhardt, *Phys. Rev. Lett.* **90**, 186403 (2003).
- [22] S. K. Mo, H. D. Kim, J. D. Denlinger, J. W. Allen, J. H. Park, A. Sekiyama, A. Yamasaki, S. Suga, Y. Saitoh, T. Muro, and P. Metcalf, *Phys. Rev. B* **74**, 165101 (2006).
- [23] J. M. Tomczak, *Spectral and Optical Properties of Correlated Materials*, PhD thesis, Ecole Polytechnique, 2007.
- [24] J. M. Tomczak and S. Biermann, *Phys. Rev. B* **80**, 085117 (2009).
- [25] L. Baldassarre, A. Perucchi, D. Nicoletti, A. Toschi, G. Sangiovanni, K. Held, M. Capone, M. Ortolani, L. Malavasi, M. Marsi, P. Metcalf, P. Postorino, and S. Lupi, *Physical Review B* **77**, 113107 (2008).
- [26] A. Perucchi, L. Baldassarre, P. Postorino, and S. Lupi, *Phys.: Condens. Matter* **21**, 323202 (2009).
- [27] K. Held, G. Nekrasov, A. Keller, V. Eyert, N. Blümer, A. K. McMahan, R. T. Scalettar, T. Pruschke, V. I. Anisimov, and D. Vollhardt, *phys. stat. sol. (b)* **56**, 829 (2007).
- [28] G. Kotliar, S. Y. Savrasov, K. Haule, V. S. Oudovenko, O. Parcollet, and C. A. Marianetti, *Reviews of Modern Physics* **78**, 865 (2006).
- [29] K. Held, *Advances in Physics* **56**, 829 – 926 (2007).
- [30] S. Lupi, L. Baldassarre, B. Mansart, A. Perucchi, A. Barinov, P. Dudin, E. Papalazarou, F. Rodolakis, J. P. Rueff, J. P. Itié, S. Ravy, D. Nicoletti, P. Postorino, P. Hansmann, N. Parragh, A. Toschi, T. Saha-Dasgupta, O. K. Andersen, G. Sangiovanni, K. Held, and M. Marsi, *Nature Communications* **1**, 105 (2010).
- [31] A. I. Frenkel, D. M. Pease, J. I. Budnick, P. Metcalf, E. A. Stern, P. Shanthakumar, and T. Huang, *Phys. Rev. Lett.* **97**, 195502 (2006).

- [32] H. Kuwamoto, J. M. Honig, and J. Appel, *Phys. Rev. B* **22**, 2626–2636 (1980).
- [33] K. D. Cummings, J. C. Garland, and D. B. Tanner, *Phys. Rev. B* **30**, 4170–4182 (1984).
- [34] T. M. Rice and W. F. Brinkman, *Phys. Rev. B* **5**, 4350–4357 (1972).
- [35] P. Limelette, A. Georges, D. Jerome, P. Wzietek, P. Metcalf, and J. M. Honig, *Science* **302**, 89–92 (2003).
- [36] M. Jarrell and J. E. Gubernatis, *Physics Reports* **269**, 133–195 (1996).
- [37] I. Solovyev, N. Hamada, and K. Terakura, *Phys. Rev. B* **53**, 7158–7170 (1996).
- [38] S. Y. Ezhov, V. I. Anisimov, D. I. Khomskii, and G. A. Sawatzky, *Phys. Rev. Lett.* **83**, 4136–4139 (1999).
- [39] K. Held, A. K. McMahan, and R. T. Scalettar, *Phys. Rev. Lett.* **87**, 276404 (2001).
- [40] G. Sangiovanni, A. Toschi, E. Koch, K. Held, M. Capone, C. Castellani, O. Gunnarsson, S. K. Mo, J. W. Allen, H. D. Kim, A. Sekiyama, A. Yamasaki, S. Suga, and P. Metcalf, *Phys. Rev. B* **73**, 205121 (2006).
- [41] A. Toschi, P. Hansmann, G. Sangiovanni, T. Saha-Dasgupta, O. K. Andersen, and K. Held, *Journal of Physics: Conference Series* **200**, 012208 (4pp) (2010).
- [42] F. Rodolakis, P. Hansmann, J. P. Rueff, A. Toschi, M. Haverkort, G. Sangiovanni, A. Tanaka, T. Saha-Dasgupta, O. Andersen, K. Held, M. Sikora, I. Alliot, J. P. Iti, F. Baudelet, P. Wzietek, P. Metcalf, and M. Marsi, *Phys. Rev. Lett.* **104**, 047401 (2010).
- [43] M. J. Rozenberg, G. Kotliar, H. Kajueter, G. A. Thomas, D. H. Rapkine, J. M. Honig, and P. Metcalf, *Phys. Rev. Lett.* **75**, 105–108 (1995).
- [44] G. L. Carr, S. Perkowitz, and D. B. Tanner, *Infrared and millimeter waves* (Academic Press, Orlando, 1985).
- [45] M. M. Qazilbash, M. Brehm, B. G. Chae, P. C. Ho, G. O. Andreev, B. J. Kim, S. J. Yun, A. V. Balatsky, M. B. Maple, F. Keilmann, H. T. Kim, and D. N. Basov, *Science* **318**, 1750 (2007).
- [46] L. Gregoratti, S. Gunther, J. Kovac, M. Marsi, R. Phaneuf, and M. Kiskinova, *Phys. Rev. B* **59**, 2018 (1999).
- [47] M. Marsi, S. L. Rosa, Y. Hwu, F. Gozzo, C. Coluzza, A. Baldereschi, G. Margaritondo, J. McKinley, S. Baroni, and R. Resta, *J. Appl. Phys.* **71**, 2048 (1992).
- [48] M. Marsi, R. Houdré, A. Rudra, M. Ilegems, F. Gozzo, C. Coluzza, and G. Margaritondo, *Phys. Rev. B* **47**, 6455 (1993).
- [49] B. Mansart, A. Barinov, P. Dudin, L. Baldassarre, A. Perucchi, E. Papalazarou, P. Metcalf, S. Lupi, and M. Marsi, *Appl. Phys. Lett.* **100**, 014108 (2012).
- [50] S. K. Mo, J. D. Denlinger, H. D. Kim, J. H. Park, J. W. Allen, A. Sekiyama, A. Yamasaki, K. Kadono, S. Suga, Y. Saitoh, T. Muro, P. Metcalf, G. Keller, K. Held, V. Eyert, V. I. Anisimov, and D. Vollhardt, *Phys. Rev. Lett.* **90**, 186403 (2003).
- [51] S. K. Mo, H. D. Kim, J. D. Denlinger, J. W. Allen, J. H. Park, A. Sekiyama, A. Yamasaki, S. Suga, Y. Saitoh, T. Muro, and P. Metcalf, *Phys. Rev. B* **74**, 165101 (2006).
- [52] F. Rodolakis, P. Hansmann, J. P. Rueff, A. Toschi, M. Haverkort, G. Sangiovanni, K. Held, M. Sikora, A. Congeduti, J. P. Itie, F. Baudelet, P. Metcalf, and M. Marsi, *Journal of Physics: Conference Series* **190**, 012092 (2009).
- [53] F. Rodolakis, J. P. Rueff, M. Sikora, I. Alliot, J. P. Iti, F. Baudelet, S. Ravy, P. Wzietek, P. Hansmann, A. Toschi, M. Haverkort, G. S. K. Held, P. Metcalf, and M. Marsi, *Phys. Rev. B* **84**, 245113 (2011).
- [54] A. Tanaka and T. Jo, *Journal of the Physical Society of Japan* **63**, 2788 (1994).
- [55] F. M. F. de Groot, *Journal of Electron Spectroscopy and Related Phenomena* **67**, 529 (1994).
- [56] T. Thole, *Journal of Electron Spectroscopy and Related Phenomena* **86**, 1 (1997).
- [57] M. W. Haverkort, Spin and orbital degrees of freedom in transition metal oxides and oxide thin films studied by soft x-ray absorption spectroscopy, PhD thesis, Universität zu Köln, 2005.
- [58] F. de Groot, *Chemical Reviews* **101**, 1779–1808 (2001).
- [59] A. Bianconi and C. R. Natoli, *Solid State Communications* **27**, 1177–1179 (1978).
- [60] J. Goulon, A. Rogalev, C. Goulon-Ginet, G. Benayoun, L. Paolasini, C. Brouder, C. Malgrange, and P. A. Metcalf, *Phys. Rev. Lett.* **85**, 4385–4388 (2000).
- [61] C. Gougoussis, M. Calandra, A. Seitsonen, C. Brouder, A. Shukla, and F. Mauri, *Phys. Rev. B* **79**, 045118 (2009).
- [62] I. S. Elfimov, N. A. Skorikov, V. I. Anisimov, and G. A. Sawatzky, *Phys. Rev. Lett.* **88**, 015504 (2001).
- [63] M. S. Laad, L. Craco, and E. Müller-Hartmann, *Phys. Rev. B* **73**, 045109 (2006).
- [64] F. Rodolakis, B. Mansart, E. Papalazarou, S. Gorovikov, P. Vilmercati, L. Petaccia, A. Goldoni, J. P. Rueff, S. Lupi, P. Metcalf, and M. Marsi, *Phys. Rev. Lett.* **102**, 066805 (2009).